Facet-Selective Deposition of Au and Pt on Ag Nanocubes for the Fabrication of Bifunctional Ag@Au-Pt Nanocubes and Trimetallic Nanoboxes

Journal:	*Nanoscale*
Manuscript ID	NR-ART-03-2018-001794.R1
Article Type:	Paper
Date Submitted by the Author:	07-Apr-2018
Complete List of Authors:	Zhang, Zhiwei; Xiamen University, Physics Ahn, Jaewan; Georgia Institute of Technology, Materials Science and Engineering Kim, Junki; Georgia Institute of Technology, Materials Science and Engineering Wu, Zhengyun; Xiamen Univ., Physics Dept. Qin, Dong; Georgia Institute of Technology, Materials Science and Engineering

SCHOLARONE™
Manuscripts

Facet-Selective Deposition of Au and Pt on Ag Nanocubes for the Fabrication of Bifunctional Ag@Au-Pt Nanocubes and Trimetallic Nanoboxes

Zhiwei Zhang,[†,‡] Jaewan Ahn,[†] Junki Kim,[†] Zhengyun Wu,[‡] and Dong Qin[†,]*

[†]School of Materials Science and Engineering, Georgia Institute of Technology, Atlanta, Georgia 30332, United States

[‡]Department of Physics, Xiamen University, Xiamen 361005, Fujian Province, P. R. China

*Corresponding author: dong.qin@mse.gatech.edu

KEYWORDS: facet-selective deposition; trimetallic nanocrystals; nanoboxes; surface-enhanced Raman scattering; localized-surface plasmon resonance

Abstract

We report a facile route to the synthesis of Ag@Au-Pt trimetallic nanocubes in which the Ag, Au, and Pt atoms are exposed at the corners, side faces, and edges, respectively. Our success relies on the use of Ag@Au nanocubes, with Ag_2O patches at the corners and Au on the side faces and edges, as seeds for the site-selective deposition of Pt on the edges only in a reaction system containing ascorbic acid (H_2Asc) and poly(vinylpyrrolidone). At an initial pH of 3.2, H_2Asc can dissolve the Ag_2O patches, exposing the Ag atoms at the corners of a nanocube. Upon the injection of H_2PtCl_6 precursor, the Pt atoms derived from the reduction by both H_2Asc and Ag are preferentially deposited on the edges, leading to the formation of Ag@Au-Pt trimetallic nanocubes. We demonstrate the use of 2,6-dimethylphenyl isocyanide as a molecular probe to confirm and monitor the deposition of Pt atoms on the edges of nanocubes through surface-enhanced Raman scattering (SERS). We further explore the use of these bifunctional trimetallic nanoparticles with integrated plasmonic and catalytic properties for *in situ* SERS monitoring the reduction of 4-nitrothiophenol by $NaBH_4$. Upon the removal of Ag *via* H_2O_2 etching, the Ag@Au-Pt nanocubes evolve into trimetallic nanoboxes with a wall thickness of about 2 nm and well-defined openings at the corners. The trimetallic nanoboxes embrace plasmon resonance peaks in the near-infrared region with potentials in biomedical applications.

Introduction

Multimetallic nanocrystals are exciting for a number of applications that include catalysis,[1-10] plasmonics,[11-14] and surface-enhanced Raman scattering (SERS).[15-18] The excitement mainly arises from the synergetic effects between different metals, which can greatly enhance the properties relative to their monometallic counterparts. For example, we have demonstrated that the deposition of a second metal such as Pt or Pd on the surface of Ag nanocrystals can integrate both plasmonic and catalytic properties in individual nanocrystals.[14-16] Many other groups have also reported the greatly enhanced reactivity/selectivity of bimetallic nanocrystals in catalysis because of the synergetic effects between different metals.[1] Among the various parameters, including composition, size, shape, and structure (solid *versus* hollow), the shape of nanocrystals plays an essential role in controlling the properties for specific applications. It is well-established that the shape of Ag or Au nanocrystals not only controls their localized surface plasmon resonance (LSPR) properties but also their performance in applications such as SERS.[11,14] On the other hand, it has become an active subject of research in recent years to enhance the activity and/or selectivity of nanocatalysts by engineering the shape of nanocrystals to ensure that the most active and/or selective facet will be presented on the surface at the greatest proportion.[19] In addition to these benefits, the presence of a well-defined, single type of facet on the surface of a catalyst will make it much easier to elucidate the reaction mechanism.[20] Taken together, there is a strong need to development methods capable of generating multimetallic nanocrystals with well-defined and controllable shapes.

Compared to the great success for both monometallic and bimetallic systems,[12, 21] there are very few reports on the preparation of trimetallic nanocrystals with well-defined shapes and morphologies. Three strategies are documented in the literature. The first one relies on the use of one-pot synthesis to generate core-shell trimetallic nanoparticles. To this end, Yamauchi and co-workers synthesized and characterized Au@Pd-Pt core-shell nanoparticles consisting of Au core, Pd inner layer, and dendritic Pt outer shell.[22,23] Han and co-workers reported the synthesis of Au@Pd-Pt core-shell nanocrystals with a well-defined Au octahedral core and Pd-Pt alloy shell.[24] The second strategy involves the use of seed-mediated co-reduction. To this end, Skrabalak and co-workers demonstrated the synthesis of Au@Pd-Ag octopods with well-defined shapes or morphologies.[25] The third strategy relies on the use of galvanic replacement reaction and Kirkendall effect to generate Ag-Au-Pd hollow nanostructures.[26] Despite these reports, it

remains elusive to fabricate trimetallic nanocrystals with the distinctive elements being exposed on different types of facets.

Herein, we report a facile approach to the synthesis of Ag@Au-Pt trimetallic nanocubes with the Au and Pt atoms being selectively exposed on the side faces and edges, respectively, of Ag nanocubes. Firstly, we use our published protocol to produce Ag@Au nanocubes with Ag_2O patches at the corners and conformal Au overlayers on the side faces and edges.[27,28] We then disperse the as-obtained nanocrystals in an aqueous solution containing ascorbic acid (H_2Asc) and poly(vinylpyrrolidone) (PVP) at pH = 3.2. Under the acid condition, the Ag_2O patches at the corners of nanocubes will be etched away by the H_2Asc,[29,30] exposing the underneath Ag atoms. When H_2PtCl_6 precursor is injected into the reaction solution, the Pt atoms derived from the reduction by Ag (*via* galvanic replacement) and H_2Asc will be preferentially deposited on the edges, or {110} facets, of the Ag@Au nanocubes, leading to the formation of Ag@Au-Pt nanocubes with the three elements exposed on different facets. We further demonstrate that the Ag@Au-Pt nanocubes embrace a strong SERS activity when used with a SERS probe such as 2,6-dimethylphenyl isocyanide (2,6-DMPI). Remarkably, this molecular probe can be used to report the deposition of Pt atoms on the edges of Ag@Au nanocubes with a sensitivity approaching monolayer. We also explore the bifunctional Ag@Au-Pt nanocubes with combined plasmonic and catalytic properties as a SERS probe for *in situ* monitoring the reduction of 4-nitrothiophenol (4-NTP) by $NaBH_4$. We identify that the reduction rate can be significantly accelerated when Ag@Au-Pt nanocubes are introduced as catalysts in comparison with the case of Ag@Au nanocubes. When the Ag cores are removed with an aqueous H_2O_2, the Ag@Au-Pt nanocubes are transformed into Ag-Au-Pt nanoboxes with a wall thickness of about 2 nm, together with well-defined openings at the corner sites. The trimetallic nanoboxes embrace strong plasmon resonance, with a major LSPR peak in the near infrared region.

Experimental

Chemicals and materials

Silver trifluoroacetate (CF_3COOAg, 98%), poly(vinylpyrrolidone) with an average molecular weight of 55,000 (PVP-55), sodium hydrosulfide hydrate ($NaHS \cdot xH_2O$), aqueous hydrochloric acid (HCl, 37%), L-ascorbic acid (H_2Asc, 99%), sodium hydroxide (NaOH, 98+%), gold(III) chloride trihydrate ($HAuCl_4 \cdot 3H_2O$, 99.9+%), chloroplatinic acid hexahydrate ($H_2PtCl_6 \cdot 6H_2O$,

37.5%), hydrogen peroxide (H_2O_2, 30 wt % in H_2O), 2,6-dimethylphenylisocyanide (2,6-DMPI, ≥98.0%), acetone (99.5+%), sodium borohydride ($NaBH_4$, 99.99%), and 4-nitrothiophenol (4-NTP, 80%) were all purchased from Sigma-Aldrich. Ethylene glycol (EG) was purchased from J. T. Baker. All chemicals were used as received. All aqueous solutions were prepared using deionized (DI) water with a resistivity of 18.2 MΩ·cm at room temperature.

Synthesis of Ag nanocubes

We followed the reported protocol to synthesize Ag nanocubes with an average edge length of 37.5 ± 1.5 nm.[31] The nanocubes were washed with acetone and DI water three times before they were redispersed in DI water for future use.

Synthesis of the Ag@Au core-shell nanocubes

In a typical synthesis, 2 mL of PVP-55 solution (1 mM) was introduced into a 23 mL glass vial, followed by the addition of 0.5 mL of H_2Asc (0.1 M), 0.5 mL of aqueous NaOH solution (0.2 M), and 0.02 mL of the aqueous suspension of Ag nanocubes (with a final concentration of 6.8×10^{10} particles per mL) under magnetic stirring. Next, 0.8 mL of aqueous $HAuCl_4$ solution (0.1 mM) was titrated into the mixture using a syringe pump at a rate of 0.02 mL min^{-1}. After the completion of titration, the product was collected by centrifugation at 6,000 rpm for 15 min and dispersed in 0.05 mL DI water for further use.

Synthesis of the Ag@Au-Pt trimetallic nanocubes

In a typical synthesis, 2 mL of PVP-55 solution (1 mM) was introduced into a 23 mL glass vial, followed by the addition of 0.5 mL of H_2Asc (0.1 M) and 0.05 mL of the as-prepared Ag@Au nanocubes (with a final concentration of 7.6×10^{10} particles per mL) under magnetic stirring for 10 min. Next, different volumes of aqueous H_2PtCl_6 solution (0.2 mM) was injected into the mixture using a pipet (10 μL for every shot at an interval of 30 sec). The reaction solution was maintained under magnetic stirring at room temperature for another 10 min once the injection had been completed. The product was collected by centrifugation at 4,600 rpm for 20 min and dispersed in DI water for further use.

Preparation of the Ag-Au nanoboxes and Ag-Au-Pt nanoboxes

We mixed 0.1 mL of the as-prepared Ag@Au nanocubes with 0.6 mL of PVP-55 (1 mM) and 0.4 mL of H_2Asc (0.1 M), and incubated for 20 min before we collected the particles by centrifugation at 5,000 rpm for 15 min. These treated Ag@Au nanocubes (0.1 mL with concentration of 7.6×10^{11} particles per mL) was then mixed with 1 mL of 3% aqueous H_2O_2 and incubated at room temperature for 2 h. The same etching protocol was also applied to Ag@Au-Pt nanocubes (0.1 mL, with a concentration of 7.6×10^{11} particles per mL) for the fabrication of Ag-Au-Pt nanoboxes. The resultant products were washed twice with water and re-dispersed in 0.5 mL of water.

Instrumentation and characterization

The UV-vis spectra were recorded using a Cary 50 spectrometer (Agilent Technologies, Santa Clara, CA). The quantitative measurement of Pt, Au and Ag contents was performed using an inductively coupled plasma mass spectrometer (ICP-MS, NexION 300Q, PerkinElmer, Waltham, MA). A routine centrifuge (Eppendorf 5430) was used for the collection and washing of samples and the preparation of the ICP-MS samples. Transmission electron microscopy (TEM) images were taken using a Hitachi HT7700 microscope (Hitachi, Tokyo, Japan) operating at 120 kV. Raman spectra were taken using a Renishaw Invia micro Raman system (Renishaw, Hoffman Estates, IL). High-resolution TEM images were taken using a F30 FEI TEM and a Hitachi HD2700 C_s-corrected microscope operated at 200 kV. The energy-dispersive X-ray spectroscopy (EDS) images were acquired from EDS detector on the HD2700. The XPS spectra were collected using a Thermo K-Alpha X ray photoelectron spectrometer (Thermo Fisher Scientific, Waltham, MA).

XPS analysis of Ag@Au-Pt nanocubes

Approximately 20 μL of the as-prepared sample suspension was drop casted on the surface of a 1×1 cm^2 silicon wafer and allowed to dry overnight under ambient conditions in air. The sample was then loaded into of a Thermo K-Alpha X ray photoelectron spectrometer and the Au4*f* (79–95 eV), Ag3*d* (360–380 eV), and Pt4*f* (65–80 eV) regions of the sample were measured with a 0.1 eV resolution.

Conversion of original EDS mapping results to line-scan data

The raw data from the EDS mapping of each element were first converted into greyscale, and the region of interest was defined to be 600 pixels long and 80 pixels tall. The line scan plot was generated by plotting the sum of all intensity values within each column of pixels (y-axis) for all 600 columns of pixels (x-axis). The raw scale bar was used to calibrate the real values for the distance of each position on the x-axis. Each data point was connected to the next with a straight line.

SERS measurements

The as-prepared Ag@Au and Ag@Au-Pt nanocubes were functionalized with a 10^{-5} M ethanol solution of 2,6-DMPI for 2 h. After washing with water twice, the 2,6-DMPI-functionalized nanoparticles were redispersed in water to attain a concentration of approximately 5.5×10^{10} particles per mL. The Raman spectra were taken using a Renishaw inVia Raman spectrometer coupled with a Leica microscope using a 100× objective. The excitation wavelength was 532 nm, in conjunction with a grating of 2400 lines per mm, at a power of 10% of the laser output (50 mW). Data was collected from the solution phase with a collection time of 10 s for all samples. A sample cell was fabricated from a polydimethylsiloxane (PDMS) block by punching a small hole to hold 20 µL of liquid sample. After the PDMS was attached to a glass slide, we loaded the sample solution and then placed a glass coverslip of 170 µm in thickness on top of the PDMS to prevent solvent evaporation.

***In situ* SERS monitoring of the reduction of 4-NTP by Ag@Au nanocubes and Ag@Au-Pt nanocubes**

The Ag@Au and Ag@Au@Pt nanocubes were dispersed in ethanol solution 4-NTP (10^{-6} M) and incubated at room temperature for 1 h. The 4-NTP-functionalized particles were then washed with DI water twice and redispersed in DI water to achieve a concentration of approximately 1.4 $\times 10^{11}$ particles per mL. Upon mixing 200 µL of the suspension with 60 or 200 µL of aqueous NaBH$_4$ (0.1 mg mL^{-1}) in a 1.5 mL centrifuge tube, the products were allowed to catalyze the 4-NTP reduction reaction at room temperature. We then withdrew 20 µL of sample from the reaction solution every several minutes and placed this sample in a PDMS based cell for collecting the SERS spectra using a 5× objective, together with a data collection time of 7 s at a power of 100% of the output of 532 nm laser (50 mW).

Results and discussion

We first prepared Ag nanocubes with an average edge length of 37.5±1.5 nm by following the published protocol (Figure S1).[31] Figure 1 shows a schematic illustration of how to transform Ag nanocubes into Ag@Au-Pt trimetallic nanocubes. In the first step, we titrate aqueous $HAuCl_4$ into an aqueous suspension of Ag nanocubes in the presence of H_2Asc (a reducing agent), PVP (a stabilizer), and NaOH (a pH modifier) at an initial pH of 11.8 using a syringe pump. Based on our published work,[30] we argue that the added $HAuCl_4$ should firstly react with the Ag atoms positioned on the {111} facets (*i.e.*, corners) of the nanocube for the deposition of Au atoms on the {110} facets (*i.e.*, edges) through a galvanic replacement mechanism. The released Ag^+ ions should react immediately with the OH^- ions for the formation of Ag_2O patches at the corners, terminating the galvanic replacement reaction. Meanwhile, the added $HAuCl_4$ undergoes ligand exchange with OH^- to form $AuCl(OH)_3^-$ and $Au(OH)_4^-$ before they are reduced by ascorbate monoanion ($HAsc^-$) to generate Au atoms for their deposition onto the entire surface of each nanocube. Combined together, Ag nanocubes are transformed into Ag@Au core-shell nanocubes, together with Ag_2O patches under the Au overlayers at the corner sites. In the second step, we disperse the as-obtained Ag@Au nanocubes in an aqueous solution containing H_2Asc and PVP under magnetic stirring for 10 min. At an initial pH of 3.2, H_2Asc can dissolve the Ag_2O patches, exposing the underlying Ag atoms at the corners. Upon the injection of aqueous H_2PtCl_6, the Pt atoms derived from the reduction of H_2PtCl_6 by both Ag and H_2Asc are selectively deposited on the edges, leading to the formation of Ag@Au-Pt trimetallic nanocubes with Ag, Au, and Pt atoms spatially confined to the {111}, {100}, and {110} facets, respectively.

Figure 2A shows a transmission electron microscopy (TEM) image of the as-obtained Ag@Au nanocubes obtained after titrating 0.8 mL of aqueous $HAuCl_4$ (see experimental section for details). The cubic shape was largely preserved in the products, while the average edge length was increased from 37.5±1.5 nm to 39.9±1.7 nm. After treating the sample with H_2Asc for 20 min and then incubating with aqueous H_2O_2 for 2 h, Figure 2B shows the formation of nanoboxes with well-defined openings at the corners, consistent with our previous findings.[30] Figure 2C shows TEM image of the Ag@Au-Pt nanocubes corresponding to the injection of 10 μL of aqueous H_2PtCl_6. Again, there was very little change to the morphology but the average edge length was further increased to 40.4±1.6 nm. After etching with aqueous H_2O_2, Figure 2D

shows a TEM image of the resultant structures, indicating the formation of nanoboxes with a cubic shape and well-defined pores at the corners. When the injection volume of H_2PtCl_6 was increased to 50 µL, Figure 2E shows a typical TEM image of the products. We noticed that the particles still took a cubic shape, with slightly sharpened corners under projection. The edge length was increased to 41.6±1.3 nm, suggesting that more Pt atoms were deposited on the edges. After treatment with aqueous H_2O_2, Figure 2F shows the formation of cubic nanoboxes similar to those shown in Figure 2D except that the edges became rougher, likely because of the deposition of more Pt atoms. To confirm the deposition of Pt on the Ag@Au nanocubes, we used ICP-MS to measure the Pt content. It was found that the amount of Pt was increased from 0.05 to 0.20 wt% as the injection volume of H_2PtCl_6 solution was increased from 10 to 50 µL. Figure S2 compares the X-ray photoelectron spectroscopy (XPS) data of these two samples. We observed an increase in the amount of Pt deposited on the Ag@Au nanocubes as the injection volume was increased, consistent with the ICP-MS results.

We also used energy dispersive X-ray spectroscopy (EDS) mapping to exam the distributions of constituent elements on an individual trimetallic nanocube. Figure 3A shows an aberration-corrected high-angle annular dark-field scanning TEM (HAADF-STEM) image taken from a trimetallic nanocube prepared with the addition of 0.8 mL of aqueous $HAuCl_4$ and 50 µL of aqueous H_2PtCl_6. When the nanocube was oriented along the ⟨001⟩ zone axis, Figure 3, B-D, shows the spatial distributions of Ag, Au, and Pt. We noticed that the distribution of Ag was confined to a solid square while Au was largely deposited around the nanocube. Under the experimental condition, it is anticipated that the amount of Au being deposited on the surface of each Ag nanocube was adequate to form a complete shell of six atomic layers thick.[27] As such, it is difficult to resolve the difference in thickness between the Au overlayers deposited on {111} and {100} facets. On the other hand, the Pt signals appeared to be slightly stronger on the edges compared to those on the side faces and corners. Based on the EDS mapping results of Ag@Au-Pt nanocube shown in Figure S3A, we performed an analysis to construct the line-scan data by defining a region of interest (see more details in the experimental session). Figure S3B shows the result of our analysis, supporting our argument that more Pt atoms would be deposited on the edges of nanocubes. Figure S3, A and B, also suggests that we could identify some Ag atoms on the outermost surface of a Ag@Au nanocube. During the deposition of Pt on Ag@Au nanocubes in presence of H_2Asc, we argue that some H_2PtCl_6 could react with Ag atoms of Ag@Au

nanocubes via galvanic replacement reaction, leading to the formation of Ag^+ ions in the reaction solution. Likely, these released Ag^+ ions and the H_2PtCl_6 could be co-reduced by H_2Asc to generate Ag atoms and Pt atoms followed by their co-deposition on Ag@Au nanocubes.

To verify the formation of Ag@Au-Pt nanocubes, we used 2,6-dimethylphenyl isocyanide (2,6-DMPI) as a molecular probe to detect the deposition of Pt on the edges of the Ag@Au nanocubes by surface-enhanced Raman scattering (SERS). In a recent study, we demonstrated the use of 2,6-DMPI for *in situ* monitoring the deposition of Pt on Ag nanocubes.[32] Because the sites for preferential heterogeneous nucleation and the SERS hot spots coincide at the edges of a Ag nanocube, this new detection paradigm allows for unprecedented sensitivity, with a lower detection limit below one monolayer. More interestingly, the stretching frequency for the NC bond would be different when the isocyanide group binds to the Ag and Pt atoms, respectively, making it feasible to characterize the Pt atoms located on the edges of Ag nanocube by following the ν_{NC} stretching frequency and the peak intensity. Figure 4 shows the SERS spectra of 2,6-DMPI adsorbed on the Ag@Au nanocubes before and after they had reacted with different volumes of H_2PtCl_6, with an excitation wavelength at 532 nm. Before the injection of H_2PtCl_6, the spectrum showed two characteristic peaks at 2177 and 648 cm^{-1}, which could be assigned to the NC stretching, $\nu_{NC(Au)}$, and C-NC stretching, $\nu_{C-NC(Au)}$, bands, respectively, of 2,6-DMPI adsorbed on Au.[33] The remaining peaks were associated with the ring-associated bands of 2,6-DMPI.[34] At a injection volume of 10 μL, in addition to the major $\nu_{NC(Au)}$ and $\nu_{C-NC(Au)}$ peaks, we resolved two new peaks at 2105 and 675 cm^{-1}, which could be assigned to the $\nu_{NC(Pt)}$ and $\nu_{C-NC(Pt)}$ bands, respectively, of 2,6-DMPI adsorbed on Pt. At 50 μL, the $\nu_{NC(Pt)}$ and $\nu_{C-NC(Pt)}$ bands became predominant with a decrease in peak intensity for both $\nu_{NC(Au)}$ and $\nu_{C-NC(Au)}$ bands, indicating more Pt atoms being deposited on the edges of the nanocubes. Taken together, this set of SERS data provided a strong evidence to support the deposition of Pt on the edges of Ag@Au nanocubes.

To further confirm the deposition of Pt, we used H_2O_2 etching to remove Ag from the sample obtained with 50 μL of H_2PtCl_6 solution. Figure 5A shows the aberration-corrected high-angle annular bright-field scanning TEM (HAABF-STEM) image of one such nanobox shown in Figure 2F. Figure 5B shows atomic-resolution HAABF-STEM image recorded from the corner region of a nanobox. We could resolve the highly ordered arrangement for the atoms on the side faces, confirming the deposition of Au on the {100} facets of the nanocube. However, it was

10

difficult to distinguish individual atoms on the edges because of the deposition of Pt to generate a Ag-Au-Pt alloy. The wall thickness of the nanobox was about 2 nm. On the other hand, as indicated by the white, dashed lines, we observed a well-defined opening at the corner from the STEM image, suggesting that exposed Ag atoms were located on the {111} facets and they could be removed during H_2O_2 etching. Figure 5C shows the STEM image of another nanobox in Figure 2F when it was oriented along the ⟨001⟩ zone axis. Figure 5, D-F, shows the spatial distributions of Ag, Au, and Pt for the same nanobox, respectively, together with openings at the corners. By using the EDS mapping data of Ag-Au-Pt nanobox shown in Figure S3C, we conducted the above-mentioned analysis to obtain line-scan data across a region of interest. Figure S3D shows that Ag, Au, and Pt were mainly confined to the edges. It is also worth mention that the EDS results show that the size of Au is slightly small than that of Ag, suggesting the presence of Ag on the surface of Au. This observation would further support our argument on the presence of Ag on the surface of Ag@Au nanocubes (see Figure S3, A and B). Our ICP-MS analysis indicated that the nanoboxes had an elemental composition of $Ag_{57}Au_{41}Pt_2$, consistent with our EDS data.

The Ag@Au-Pt nanocubes could serve as an *in situ* SERS probe for monitoring the reduction of 4-nitrothiophenol (4-NTP) to 4-aminothiophenol (4-ATP). In a typical process, we functionalized the as-prepared nanoparticles with 4-NTP and collected SERS spectra at different time points. Figure 6A shows the SERS spectra captured during the reaction as it was catalyzed by Au@Au nanocubes. At $t = 0$, we identified three characteristic bands of 4-NTP located at 1110, 1338, and 1572 cm^{-1} (labeled by red dashed lines), corresponding to the C-N stretching (v_{CN}), O-N-O stretching (v_{NO2}), and C-C stretching (v_{CC}), respectively. The peak located at 1080 cm^{-1} could be assigned to the C-S stretching (v_{CS}). At $t = 10$ min, the v_{NO_2} of 4-NTP was red-shifted from 1338 to 1333 cm^{-1}, together with a decrease in its intensity. Also, the intensities of v_{CN} and v_{CC} bands were decreased while the peak positions remained essentially the same. At this time point, a new band emerged at 1595 cm^{-1}, which can be assigned to v_{CC} of 4-ATP (marked by a blue dashed line). As the reaction progressed to 15 min and then 20 min, we noticed that the v_{NO_2} of 4-NTP started to decrease in intensity, together with a slight shift to the blue. During this period, the v_{CC} of 4-NTP was continuously decreased in intensity as that of 4-ATP was gradually increased in intensity. At $t = 25$ min, three bands associated with 4-NTP all disappeared while the v_{CC} band of 4-ATP remained, indicating the completion of reaction. It is worth noting that the

peak of ν_{CS} at 1083 cm^{-1} was relatively stable during the course of the reaction, suggesting the molecules likely remained on the surface because of thiolate bonding. It is also worth mentioning that the intensity of the band at 1595 cm^{-1} for 4-ATP was 15 times weaker than the band at 1572 cm^{-1} for 4-NTP. This result suggests the desorption of 4-ATP from the surface of nanocubes because of a strong binding of BH$_4^-$ to the surface of the nanocubes.[35]

Figure 6B shows the time-elapsed SERS spectra using the Ag@Au-Pt nanocubes (obtained with 10 μL of H$_2$PtCl$_6$ solution) as the catalyst while keeping all other experimental parameters the same. At $t = 0$ min, we observed a 65% decrease in intensity for the 4-NTP peak at 1572 cm^{-1} (ν_{CC}) relative to the case of Ag@Au nanocubes. We suspected that the deposition of Pt atoms on the edges of Ag-Au nanocubes could deteriorate the SERS activity of Au.[32] Such a decrease could also arise from the less efficient adsorption of 4-NTP molecules on the Pt surface. When the reaction progressed to 3 and then 5 min after the addition of NaBH$_4$, we observed the gradual decrease in peak intensity for all three 4-NTP bands, indicating the reduction of 4-NTP to 4-ATP. However, it was difficult to resolve the ν_{CC} band of 4-ATP at 1595 cm^{-1} because of desorption of 4-ATP from the surface in the presence of BH$_4^-$, consistent with the results shown in Figure 6A. At $t = 7$ min, the spectrum only showed one small peak at 1083 cm^{-1} (νCS), indicating the completion of reaction. Taken together, we argue that the introduction of a small amount of Pt to the surface of the Ag@Au nanocubes would significantly accelerate the reduction of 4-NTP by NaBH$_4$. In order to confirm the production of 4-ATP, we performed another control experiment by adding 60 μL of NaBH$_4$ solution (0.1 mg/mL) to initiate the reaction. Figure S4 shows the SERS spectra collected at 20 min by benchmarking against those in the absence of NaBH$_4$ and the presence of NaBH$_4$ at 200 μL, respectively. When we decreased the amount of NaBH$_4$ involved to reduce the reaction rate, we were able to observe the ν_{CC} band of 4-ATP at 1595 cm^{-1}, confirming the reduction of 4-NTP to 4-ATP by NaBH$_4$ on the surface of Ag@Au-Pt nanocubes. Taken together, we believe that Ag@Au-Pt nanocubes are better catalysts for the reduction of 4-NTP by NaBH$_4$ compared with Ag@Au nanocubes.

We also used UV-vis-NIR spectroscopy to characterize the optical properties of the as-obtained Ag@Au-Pt nanocubes and the resultant nanoboxes after etching with aqueous H$_2$O$_2$. Figure 7A shows that the major LSPR peak of the Ag nanocubes was red-shifted from 428 to 438 nm for Ag@Au nanocubes upon the reaction with 0.8 mL of HAuCl$_4$ solution, followed by another slight red-shift to 444 nm after the reaction of the Ag@Au nanocubes with 50 μL

H_2PtCl_6 solution. These results suggest that the LSPR properties of the Ag nanocubes were largely preserved in both the Ag@Au and Ag@Au-Pt nanocubes. When the solid nanoparticles were transformed into nanoboxes through the removal of Ag, Figure 7B indicates that the LSPR peaks of the resultant Ag-Au and Ag-Au-Pt nanoboxes were significantly red-shifted to 1070 and to 1090 nm, respectively.

Conclusions

In summary, we demonstrated the transformation of Ag nanocubes into of Ag@Au-Pt trimetallic nanocubes with Ag, Au, and Pt surface atoms enclosed on the {111}, {100}, and {110} facets of nanocubes, respectively. In a typical process, we started with Ag nanocubes to prepare for Ag@Au nanocubes with Ag_2O patches on the {111} facets and Au on the {100} and {110} facets of nanocubes. Next, we dispersed as-obtained Ag@Au nanocubes to an aqueous solution containing H_2Asc and PVP at pH = 3.2. Under an acidic condition, H_2Asc could dissolve these Ag_2O patches, making it possible for the underlying Ag atoms exposed on the {111} facets of nanocubes. After the injection of different amount of aqueous H_2PtCl_6 to the reaction solution, the added Pt precursor would be reduced by Ag *via* galvanic replacement reaction and by H_2Asc *via* chemical reduction for the generation of Pt atoms, followed by their preferentially deposition on the {110} facets of nanocubes. As a result, the Ag@Au nanocubes were further converted into Ag@Au-Pt trimetallic nanocubes with well-defined facets enclosed by Ag, Au, and Pt atoms. We evaluated the SERS activities of Ag@Au-Pt nanocubes by using 2,6-DMPI as a molecular probe to report the Pt atoms being deposited on the edges of Ag@Au nanocubes where the SERS hot spots are located. We further demonstrated the use of these trimetallic nanoparticles with integrated plasmonic and catalytic properties for *in situ* monitoring the reduction of 4-NTP by $NaBH_4$ using SERS. After the removal of Ag in an aqueous H_2O_2, we transformed the trimetallic nanocubes into Ag-Au-Pt nanoboxes with wall thickness of ~ 2 nm and well-defined openings at the corners. These Ag-Au-Pt nanoboxes embrace strong plasmonic property with a major LSPR peak located at near infrared region.

Acknowledgement

Notes and References

(1) H.-L. Jiang and Q. Xu, *J. Mater. Chem.*, 2011, **21**, 13705-13725.

(2) H. Zhang, M. Okumura and N. Toshima, *J. Phys. Chem. C*, 2011, **115**, 14883-14891.

(3) V. Mazumder, M. Chi, K. L. More and S. Sun, *J. Am. Chem. Soc.*, 2010, **132**, 7848-7849.

(4) C. Wang, D. Van Der Vliet, K. L. More, N. J. Zaluzec, S. Peng, S. Sun, H. Daimon, G. Wang, J. Greeley, J. Pearson, A. P. Paulikas, G. Karapetrov, D. Strmcnik, N. M. Markovic and V. R. Stamenkovic, *Nano Lett.*, 2010, **11**, 919-926.

(5) P.-P. Fang, S. Duan, X.-D. Lin, J. R. Anema, J.-F. Li, O. Buriez, Y. Ding, F.-R. Fan, D.-Y. Wu and B. Ren, *Chem. Sci.*, 2011, **2**, 531-539.

(6) X. Sun, X. Yang, Y. Zhang, Y. Ding, D. Su and D. Qin, *Nanoscale*, 2017, **9**, 15107-15114.

(7) J. Li, X. Sun and D. Qin, *ChemNanoMat*, 2016, **2**, 494-499.

(8) J. W. Hong, S. W. Kang, B.-S. Choi, D. Kim, S. B. Lee and S. W. Han, *ACS nano*, 2012, **6**, 2410-2419.

(9) B. Lim, M. Jiang, P. H. Camargo, E. C. Cho, J. Tao, X. Lu, Y. Zhu and Y. Xia, *Science*, 2009, **324**, 1302-1305.

(10) Z. Peng and H. Yang, *J. Am. Chem. Soc.*, 2009, **131**, 7542-7543.

(11) M. Rycenga, C. M. Cobley, J. Zeng, W. Li, C. H. Moran, Q. Zhang, D. Qin and Y. Xia, *Chem. Rev.*, 2011, **111**, 3669-3712.

(12) K. D. Gilroy, A. Ruditskiy, H.-C. Peng, D. Qin and Y. Xia, *Chem. Rev.*, 2016, **116**, 10414-10472.

(13) J. Ahn, D. Wang, Y. Ding, J. Zhang and D. Qin, *ACS nano*, 2018, **12**, 298-307.

(14) Y. Wu, X. Sun, Y. Yang, J. Li, Y. Zhang and D. Qin, *Acc. Chem. Res.*, 2017, **50**, 1774-1784.

(15) J. Li, J. Liu, Y. Yang and D. Qin, *J. Am. Chem. Soc.*, 2015, **137**, 7039-7042.

(16) J. Li, Y. Wu, X. Sun, J. Liu, S. A. Winget and D. Qin, *ChemNanoMat*, 2016, **2**, 786-790.

(17) J. Zhang, S. A. Winget, Y. Wu, D. Su, X. Sun, Z.-X. Xie and D. Qin, *ACS nano*, 2016, **10**, 2607-2616.

(18) Y. Wu, D. Su and D. Qin, *ChemNanoMat*, 2017, **3**, 245-251.

(19) S. Xie, S.-I. Choi, X. Xia and Y. Xia, *Curr. Opin. Chem. Eng.*, 2013, **2**, 142-150.

(20) B. Roldan Cuenya, *Acc. Chem. Res.*, 2013, **46**, 1682-1691.

(21) S. Khanal, G. Casillas, J. J. Velazquez-Salazar, A. Ponce and M. Jose-Yacaman, *J. Phys. Chem. C*, 2012, **116**, 23596-23602.

(22) L. Wang and Y. Yamauchi, *Chem. Mater.*, 2011, **23**, 2457-2465.

(23) L. Wang and Y. Yamauchi, *J. Am. Chem. Soc.*, 2010, **132**, 13636-13638.

(24) S. W. Kang, Y. W. Lee, Y. Park, B.-S. Choi, J. W. Hong, K.-H. Park and S. W. Han, *ACS Nano*, 2013, **7**, 7945-7955.

(25) R. G. Weiner and S. E. Skrabalak, *Chem. Mater.*, 2016, **28**, 4139-4142.

(26) E. González, J. Arbiol and V. F. Puntes, *Science*, 2011, **334**, 1377-1380.

(27) Y. Yang, J. Liu, Z.-W. Fu and D. Qin, *J. Am. Chem. Soc.*, 2014, **136**, 8153-8156.

(28) X. Sun, Y. Yang, Z. Zhang and D. Qin, *Chem. Mater.*, 2017, **29**, 4014-4021.

(29) H. L. Johnston, F. Cuta and A. B. Garrett, *J. Am. Chem. Soc.*, 1933, **55**, 2311-2325.

(30) X. Sun, J. Kim, K. D. Gilroy, J. Liu, T. A. F. König and D. Qin, *ACS Nano*, 2016, **10**, 8019-8025.

(31) Q. Zhang, W. Li, L.-P. Wen, J. Chen and Y. Xia, *Chem. - Eur. J.*, 2010, **16**, 10234-10239.

(32) Y. Zhang, J. Liu, J. Ahn, T.-H. Xiao, Z.-Y. Li and D. Qin, *ACS Nano*, 2017, **11**, 5080-5086.

(33) K. Kim, K. L. Kim, J.-Y. Choi, H. B. Lee and K. S. Shin, *J. Phys. Chem. C*, 2010, **114**, 3448-3453.

(34) S.-W. Joo, W.-J. Kim, W. S. Yun, S. Hwang and I. S. Choi, *Appl. Spectrosc.*, 2004, **58**, 218-223.

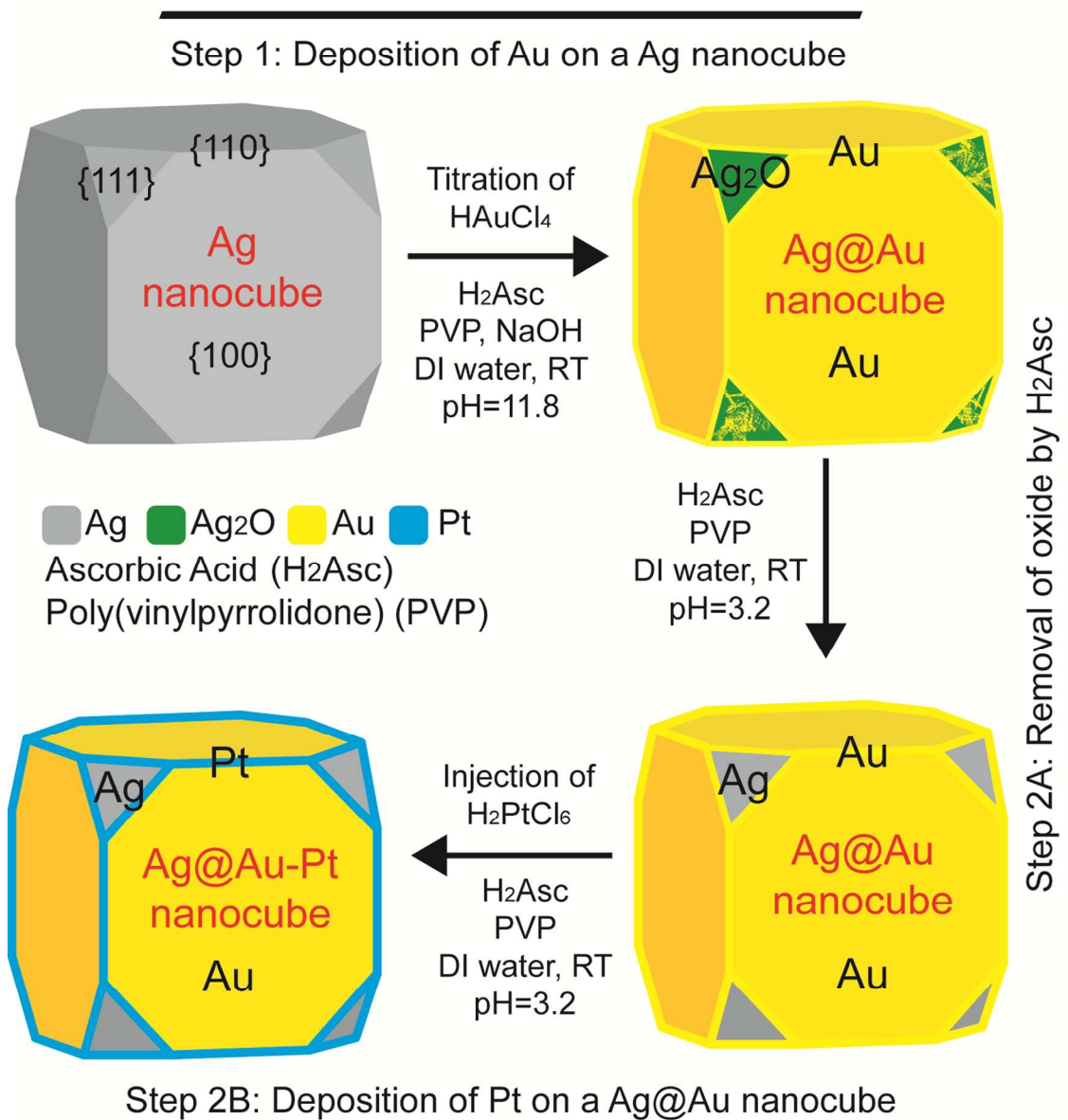(35) S. M. Ansar, F. S. Ameer, W. Hu, S. Zou, C. U. Pittman and D. Zhang, *Nano Lett.*, 2013, **13**, 1226-1229.

Figure 1. Schematic illustration of a proposed pathway responsible for the transformation of a Ag nanocube into a Ag@Au core-shell nanocube and then a Ag@Au-Pt nanocube.
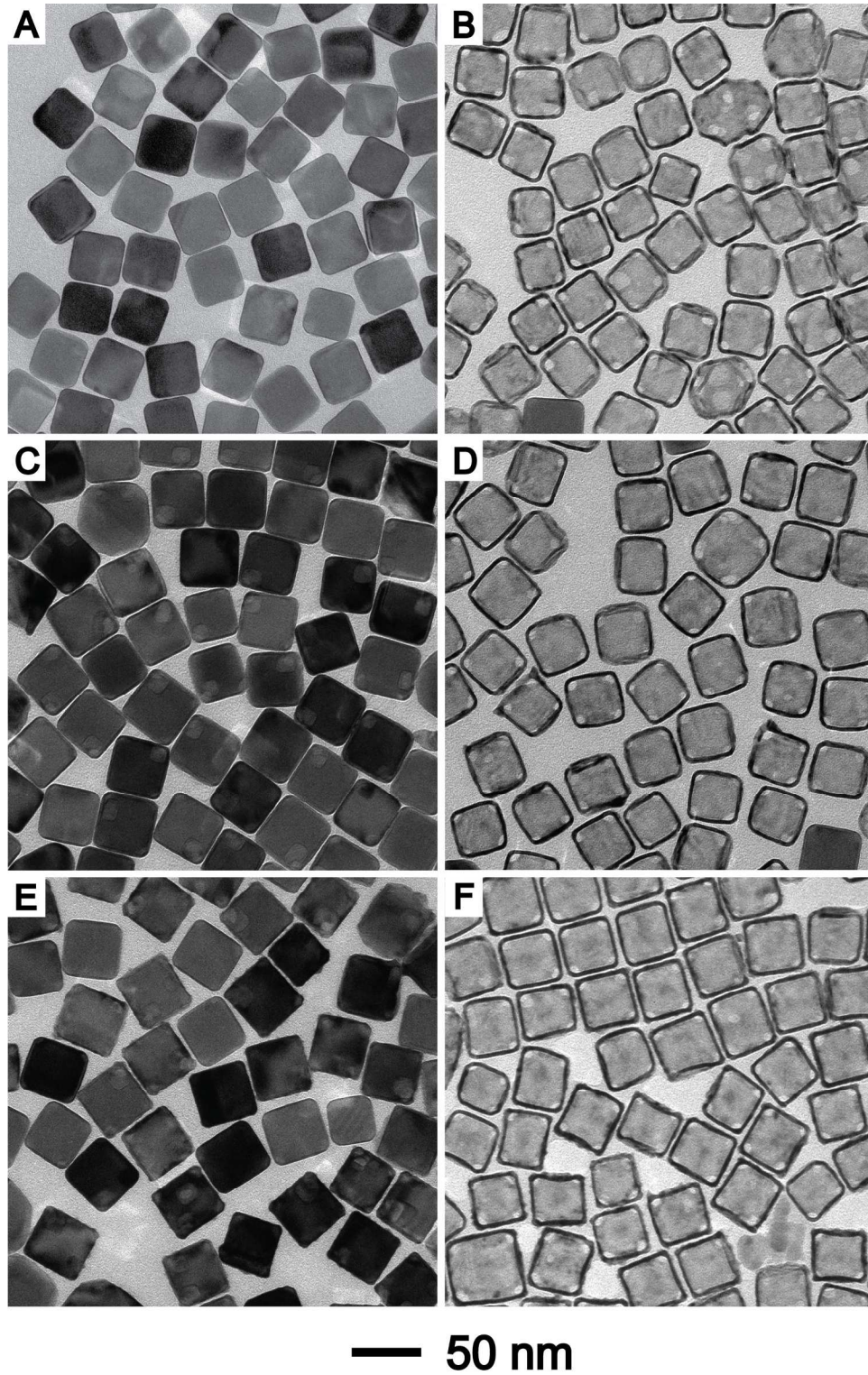
Figure 2. TEM images of (A) Ag@Au nanocubes and (C, E) Ag@Au nanocubes after reaction with (C) 10 µL and (E) 50 µL volumes of 0.2 mM aqueous H_2PtCl_6. (B, D, F) TEM images of the products after etching the samples in (A, C, E) with 3% aqueous H_2O_2.
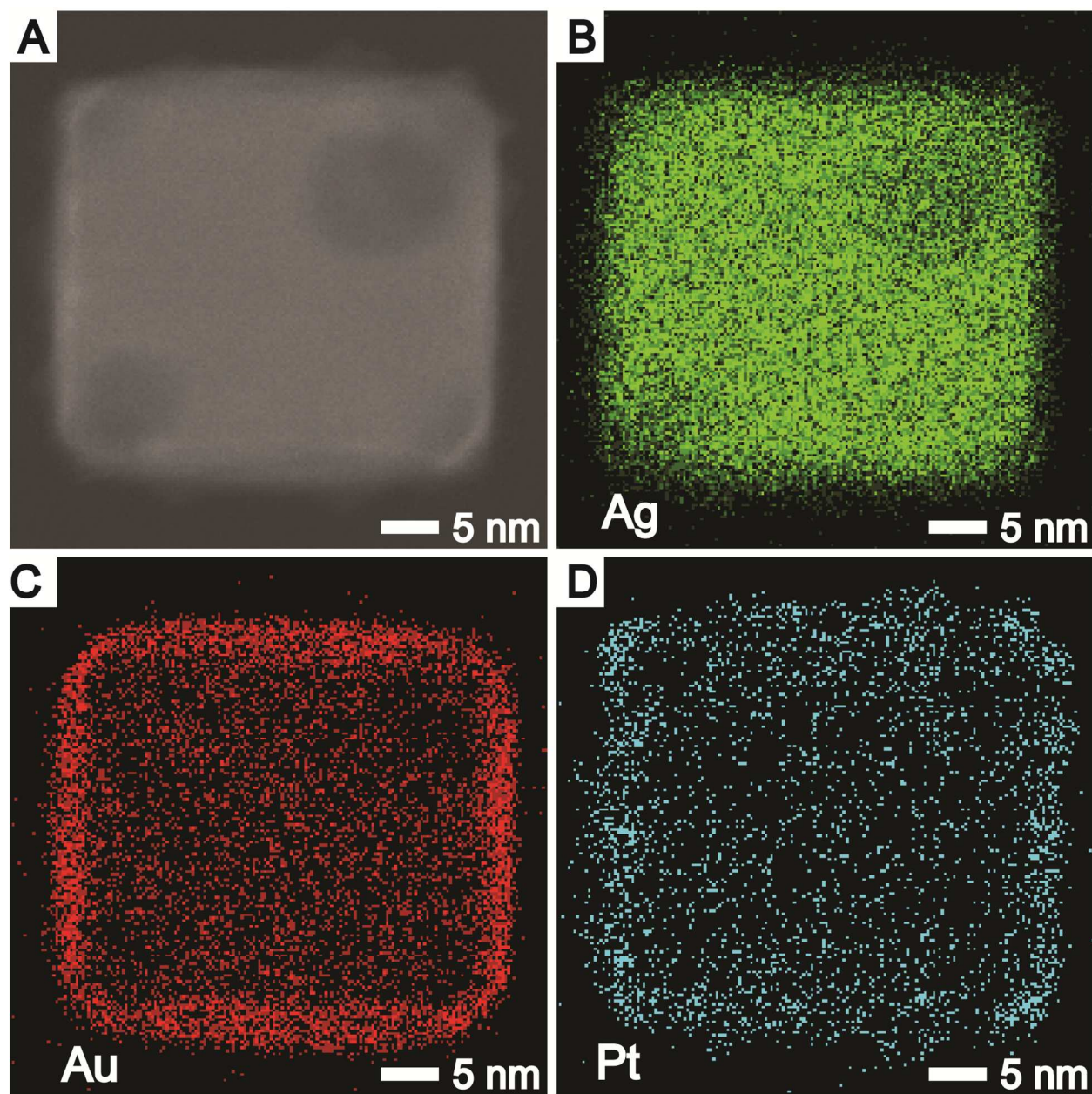
Figure 3. (A) HAADF-STEM image recorded from one of the Ag@Au-Pt nanocubes prepared with the introduction of 50 μL of aqueous H_2PtCl_6 (Fig. 2E), with the particle being orientated along the <001> zone axis. (B-D) EDS mapping of the same nanocube (green: Ag; red: Au; blue: Pt).
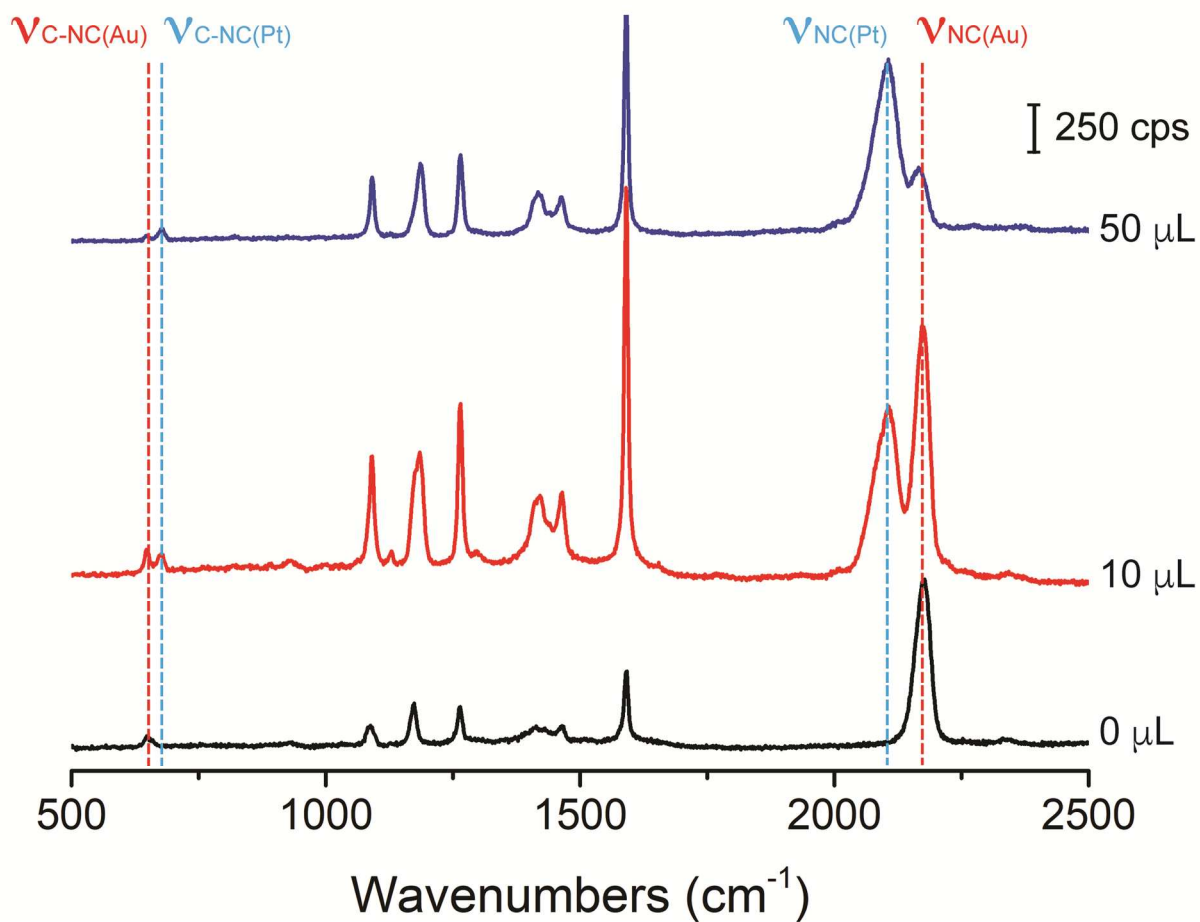
Figure 4. SERS spectra recorded from aqueous suspensions of 2,6-DMPI-functionalized samples prepared by reacting the Ag@Au nanocubes with different volumes of aqueous H_2PtCl_6.
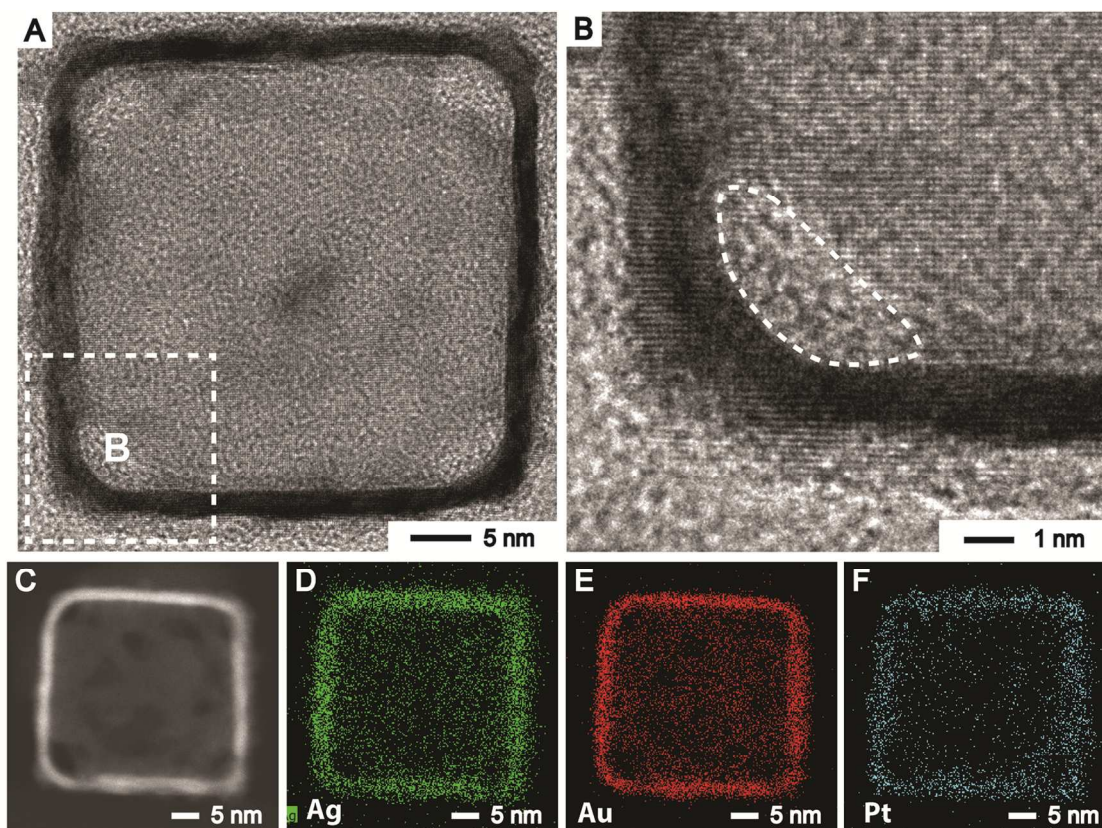
Figure 5. (A) HAABF-STEM image taken from one of the Ag@Au-Pt nanoboxes shown in Figure 2F, with the particle orientated at the <001> zone axis. (B) Atomic-resolution HAABF-STEM image taken from the corner region of a nanobox (marked by the white dashed box). (C-F) STEM image and EDX mapping of Ag (green), Au (red), and Pt (blue) for an individual nanobox shown in (C).
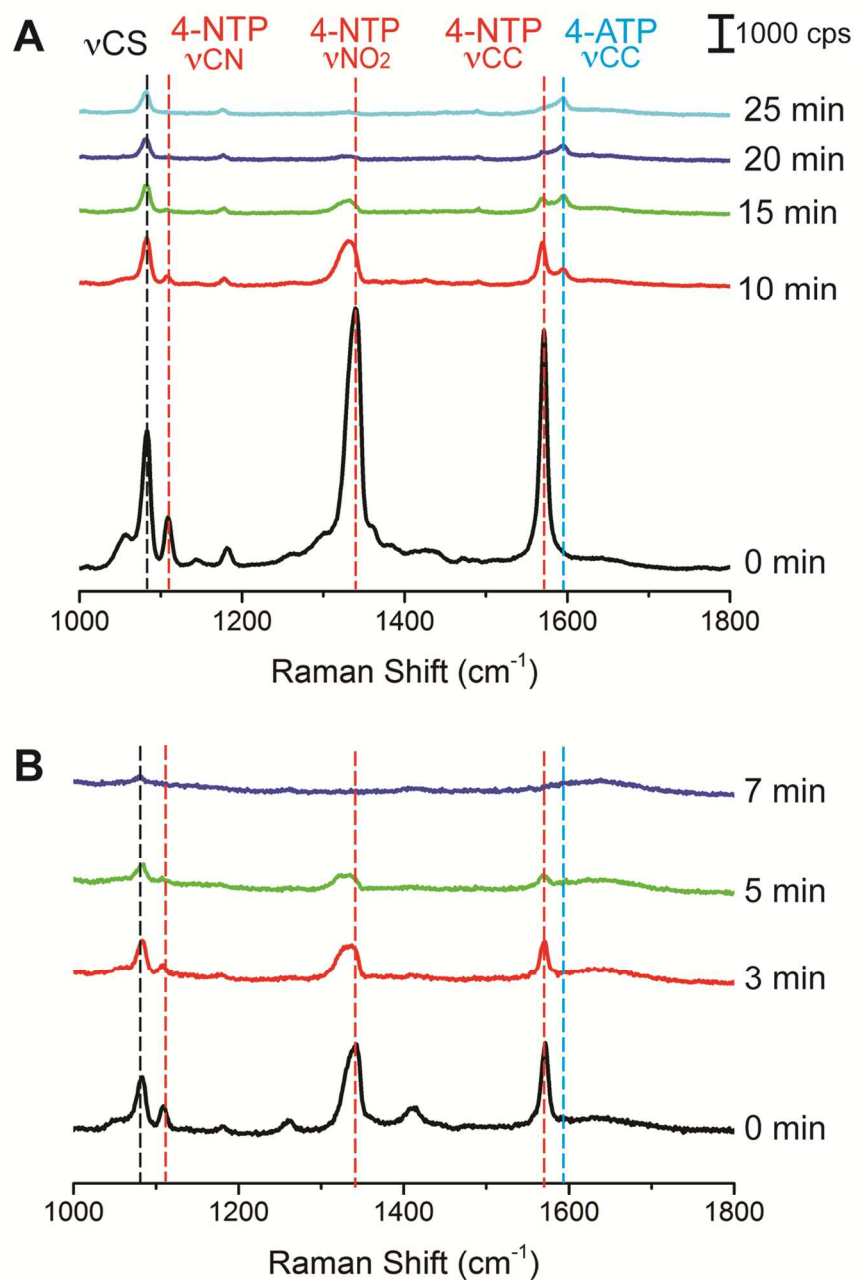
Figure 6. SERS spectra recorded during the reduction of 4-NTP to 4-ATP by 200 µL of 0.1 mg/mL NaBH$_4$ using (A) Ag@Au and (B) Ag@Au-Pt nanocubes, respectively, as the catalysts.
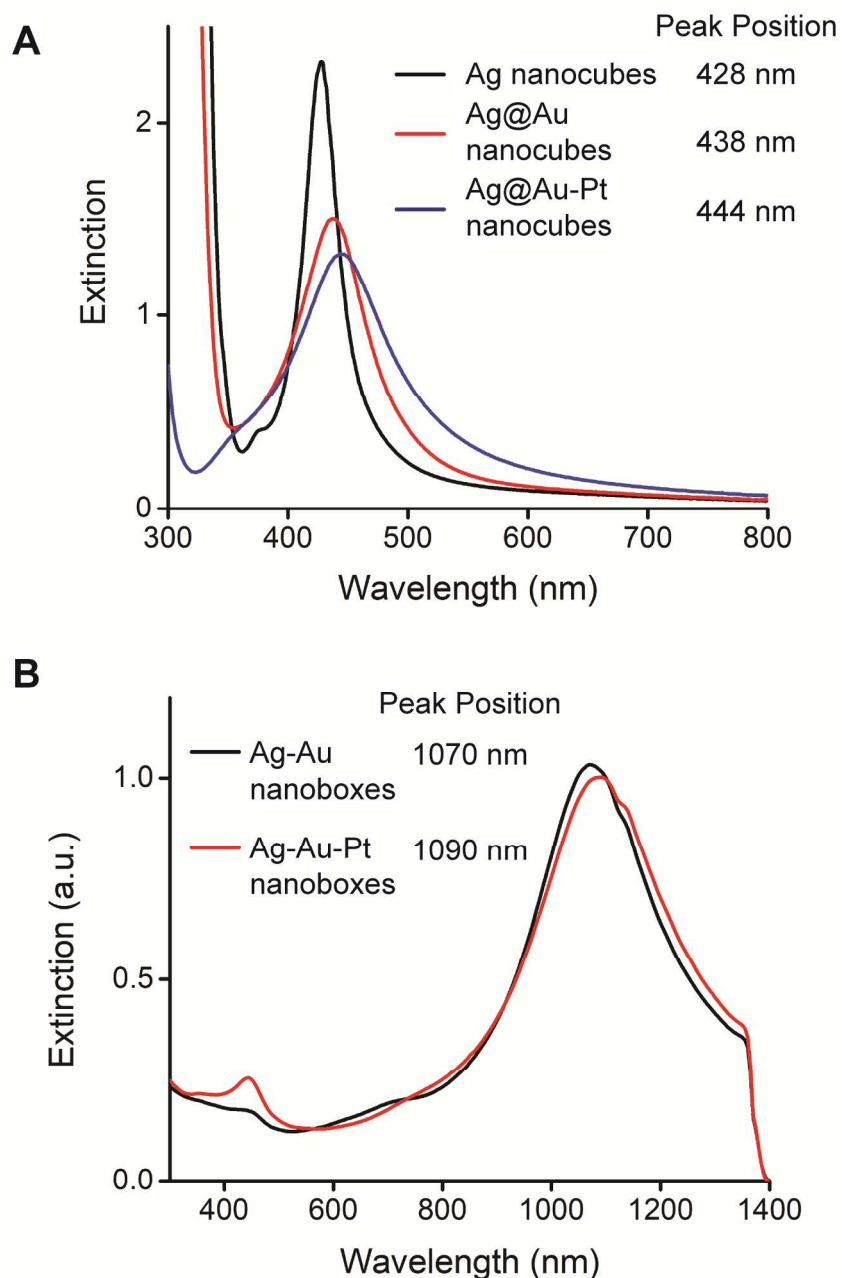
Figure 7. (A) UV-vis spectra of the Ag nanocubes, Ag@Au nanocubes prepared with 0.8 mL of HAuCl$_4$, and Ag@Au-Pt trimetallic nanocubes prepared with 0.8 mL of HAuCl$_4$ and then 50 μL of H$_2$PtCl$_6$. (B) UV-vis-NIR spectra recorded from aqueous suspensions of the resultant Ag-Au and Ag-Au-Pt nanoboxes after etching of the Ag@Au and Ag@Au-Pt nanocubes shown in (A) with 3% aqueous H$_2$O$_2$.

TOC